Fermi Surface of Beryllium and Its Pressure Dependence*

J. H. TRIPP,† P. M. EVERETT,‡ AND W. L. GORDON
Department of Physics, Case Western Reserve University, Cleveland, Ohio 44106

AND

R. W. STARK§
Department of Physics, The James Franck Institute, The University of Chicago, Chicago, Illinois

(Received 18 November 1968)

The Fermi surface of beryllium has been thoroughly investigated by means of the de Haas–van Alphen effect, and the frequencies, though substantially in agreement with earlier measurements, have been obtained to greater accuracy. This has made it possible to construct a nonlocal pseudopotential model for the Fermi surface, in which the Fourier coefficients of the crystal potential are treated as parameters to be evaluated by fitting to the experimental data. In this way, all the principal cross sections of the surface have been fitted to within 1%, using only five adjustable parameters. Comparison of calculated cyclotron masses for these cross sections with the masses determined from the temperature dependence of the dHvA amplitudes indicates that the mass is enhanced about 20% by many-body interactions neglected in the model. Finally, the pressure dependence of the Fermi surface has been calculated and compared with some available experimental measurements.

I. INTRODUCTION

THERE have been several recent studies of the Fermi surface of hcp beryllium, and the general features of these investigations, both theoretical[1–3] and experimental,[4–6] are in good agreement. A consistent picture of the Fermi surface emerges, which, however, lacks somewhat in precision. The justification for a further detailed investigation of this metal is twofold. First, on the experimental side there is a need to complete the de Haas–van Alphen (dHvA) frequency measurements to a uniform accuracy and also to provide cyclotron mass values as a function of magnetic-field direction. From the theoretical aspect there is great value in having an extremely accurate and, at the same time, soluble model for the band structure and Fermi surface. Once such a model has been obtained, it may be used to understand changes in band structure brought about either by alloying or by straining the pure metal, for example, by applying hydrostatic pressure.

It is shown in this paper how the Fermi surface can be described by a semiempirical nonlocal pseudopotential model. The parameters of the model are Fourier components of the local part of the pseudopotential and are evaluated by comparing calculated dHvA frequencies with the new observed values. Using only five parameters, the over-all accuracy of this frequency fitting for pure beryllium is better than 1% in the principal symmetry directions. A preliminary account of this work has already been published.[7] The Fermi surface is illustrated in Fig. 1 which has been drawn to be consistent with the results of the pseudopotential model. Several important cross sections are shown in Fig. 2. This surface shows a severe distortion from the nearly free-electron model, in contrast to magnesium.[8]

In Sec. II a description of the experimental measurements of the dHvA frequencies and associated effective masses in the unstrained lattice is given. The formal pseudopotential expressions for computing energy levels in the crystal are set up in Sec. III while Sec. IV indicates how these are actually used to calculate dHvA frequencies and cyclotron masses. In Sec. V the results are discussed and compared with those of other authors.

Finally, the model is generalized to the case of the strained lattice and the calculated strain and pressure derivatives of the dHvA frequencies are compared with some available experimental data. In view of the difficulty, both theoretical and experimental, in obtaining these derivatives, the present agreement between the two is surprisingly good. The application of the model to the alloy problem will be the subject of a further paper.

II. EXPERIMENTAL RESULTS

Both the field modulation and torque methods have been used in measuring the dHvA effect in the field of a 23-kG rotatable iron magnet. The field modulation magnetometer has also been used with a 60-kG superconducting solenoid. The torque magnetometer, used for some of the low-frequency neck oscillations, has

* Supported in part by the Air Force Office of Scientific Research under Grant No. AF AFOSR 536-66 to Case Western Reserve University and by the Army Research Office, Durham under Grant No. ARO-D-31-124-G926 to the University of Chicago.

† Present address: Department of Physics, University of Connecticut, Storrs, Conn.

‡ NASA Predoctoral Trainee. Present address: Department of Physics, The Louisiana State University, Baton Rouge, La.

§ Alfred P. Sloan Research Fellow.

[1] T. L. Loucks and P. H. Cutler, Phys. Rev. **133**, A819 (1964).

[2] T. L. Loucks, Phys. Rev. **134**, A1618 (1964).

[3] J. H. Terrell, Phys. Rev. **149**, 526 (1966).

[4] B. R. Watts, Phys. Letters **3**, 284 (1963).

[5] B. R. Watts, Proc. Roy. Soc. (London) **A282**, 521 (1964).

[6] R. W. Genberg, Bull. Am. Phys. Soc. II **7**, 584 (1962); thesis, Case Institute of Technology, 1965 (unpublished).

[7] J. H. Tripp, W. L. Gordon, P. M. Everett, and R. W. Stark, Phys. Letters **26A**, 98 (1967).

[8] R. W. Stark, Phys. Rev. **162**, 589 (1967).

been described earlier.[9] The large amplitude field modulation magnetometer used was very similar to those described previously.[10,11] In this method, the amplitude of the modulation field at any field orientation was adjusted either to enhance the amplitude of a particular frequency or to reduce that of unwanted frequencies. The single crystals used had residual resistance ratios of approximately 1000 and were obtained from Nuclear Metals, Inc.[12]

The dHvA frequencies and cyclotron masses are in general agreement with those of Watts[5] but have been measured with the higher precision needed to obtain the pseudopotential model parameters. Absolute accuracies for the dHvA frequencies are $\frac{1}{2}\%$ or better while those of the cyclotron masses are better than 3%. The dHvA frequencies are shown in Figs. 3 and 4 and are listed for particular directions in Sec. V, together with the cyclotron masses. Greek letters are used to denote the frequency branches arising from a common portion of the Fermi surface, with a subscript specifying the crystalline plane in which the magnetic field **H** lies [1 for $(10\bar{1}0)$, 2 for $(11\bar{2}0)$, and 3 for (0001)] and a superscript denoting the branch. α refers to the cigars, while β and γ refer, respectively, to the belly and neck of the coronet. Figure 5 illustrates typical β and γ orbits for **H** in the (0001) plane. It is also convenient to introduce the polar angle θ measured from $\langle 0001 \rangle$ in either plane, and the azimuthal angle ϕ measured from $\langle 10\bar{1}0 \rangle$.

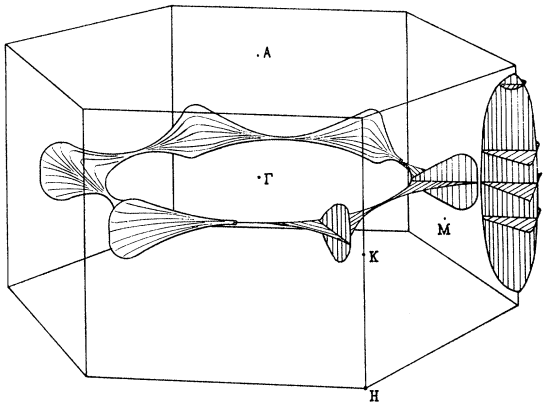

FIG. 1. Second-band hole surface (coronet) and one-half of the third-band electron surface (cigar) of beryllium. The volumes of electrons and holes are equal, about 0.8% of the volume of the first Brillouin zone or 0.016 states per atom. The shape of the cigar changes smoothly from a triangular cylinder near the ΓKM plane to a hemispherical cap just below H. There are two extremal cross sections normal to the (0001) axis; the triangular waist in the ΓKM plane is minimal while just over one quarter of the distance from K to H there is a slightly rounded triangular maximal orbit. The six large pieces of the coronet, sometimes called bellies, are disposed about the ΓK lines and joined by thin, almost cylindrical necks.

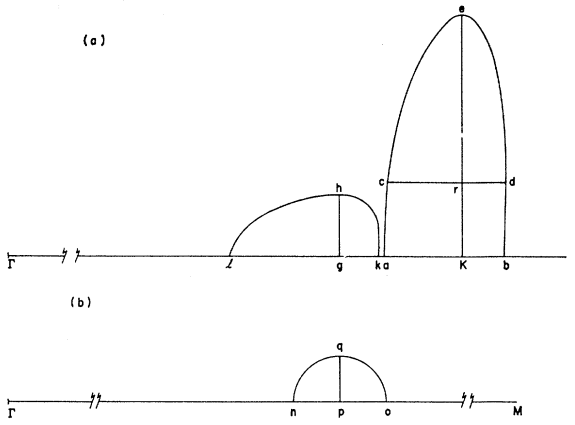

FIG. 2. Intersections of the Fermi surface with the ΓKHA and ΓMLA planes. Important caliper dimensions are labeled for later reference. The scale of (b) is 8 times that of (a).

The dHvA frequencies have been measured in two ways: by sweeping H at a given orientation and by rotating the direction of a constant H. The starting and ending fields for the γ field sweeps, which were below 10 kG, were determined from a Hall probe voltage calibrated by nuclear magnetic resonance. The small number of oscillations in the γ field sweeps, about 35, made the uncertainty in these frequencies the highest. The starting and ending fields for the β field sweeps with **H** in the basal plane were also determined from the Hall probe. However, for **H** in the $(11\bar{2}0)$ and $(10\bar{1}0)$ planes the number of β oscillations between two values of H were compared to the number of oscillations of the dominant α frequency (α^2) with **H** along [0001] in the same field interval.[13] This α frequency has been very accurately measured by O'Sullivan and Schirber[14] ($\pm 0.1\%$) and checks well with our Hall probe calibration. The β frequencies at all symmetry directions and the α frequencies at selected angles were determined by comparison with this α frequency. The frequencies at directions between those determined by the field sweep method were measured by rotating H at a constant value. The frequency difference between any two field directions is then the product of H with the number of dHvA oscillations occurring in the angular interval. The λ^1 frequency, assigned to the inside ring of the coronet by Watts, was not observed. Since the homogeneity of the magnet field at 60 kG was adequate to observe this expected frequency of 394×10^6 G, we must attribute its absence to a combination of low amplitude (a narrow band of orbits and a relatively large cyclotron mass) with a narrow angular range of occurrence. This frequency, in any case, is of little use

[9] A. S. Joseph and W. L. Gordon, Phys. Rev. **126**, 489 (1962).
[10] R. W. Stark and L. R. Windmiller, Cryogenics **8**, 272 (1968).
[11] A. Goldstein, S. J. Williamson, and S. Foner, Rev. Sci. Instr. **36**, 1356 (1965).
[12] Distilled, zone-refined material prepared by Nuclear Metals, Inc., and supplied to us through the U. S. Air Force Office of Scientific Research and the U. S. Atomic Energy Commission.
[13] If more than one frequency is present, corrections must be made to eliminate the error which occurs when a nonintegral number of the beats is compared with an integral number of [0001] α beats.
[14] W. J. O'Sullivan and J. E. Schirber, Cryogenics **7**, 118 (1967).

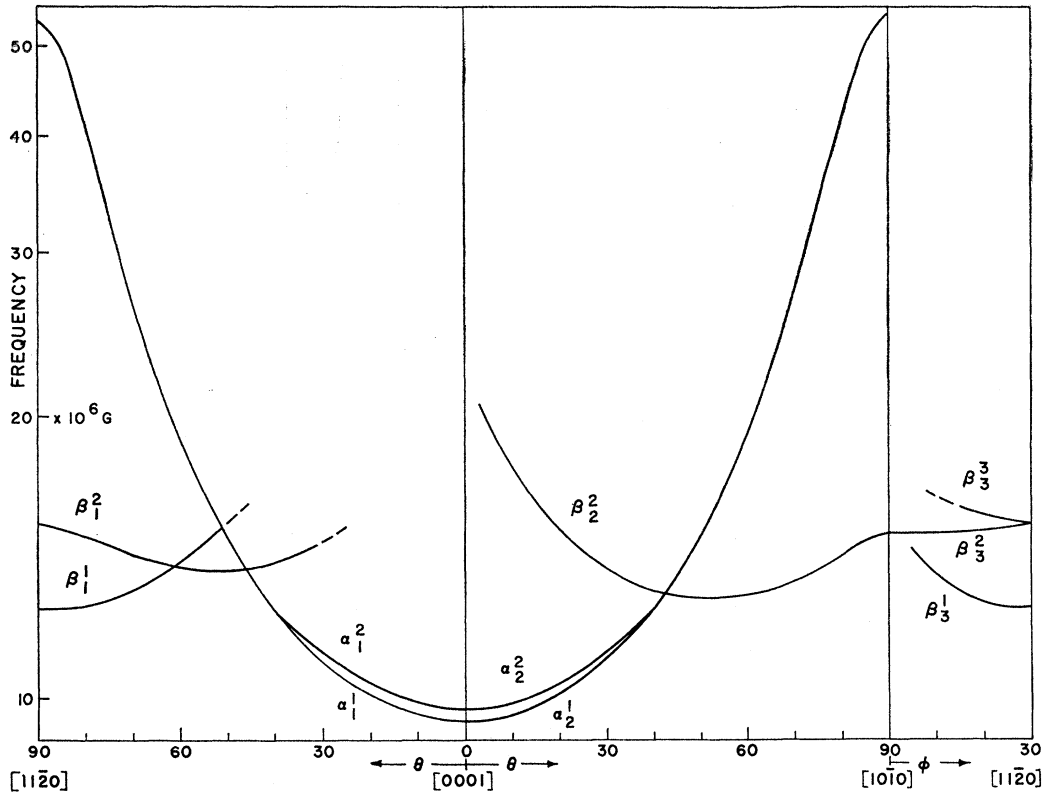

FIG. 3. Semilog plot of the angular dependence of two families of dHvA frequencies corresponding to extremal orbits on the "cigar" and on the "belly" of the coronet shown in Fig. 1.

in fitting our pseudopotential model. In common with Watts, the outer orbit on the coronet λ^2 was not observed.

The γ frequencies varying as the secant of the angle of rotation, show that the neck is cylindrical near $\langle 11\bar{2}0\rangle$. At 30° from $\langle 11\bar{2}0\rangle$ in both the (0001) plane and the $(10\bar{1}0)$ plane the secant has been exceeded by less than $\frac{1}{2}\%$. At 60° from $\langle 11\bar{2}0\rangle$ the γ_3^2 frequency has risen only 2.8% above secant behavior, and γ_1^1 only 3.9%. No sharp cutoff in the γ frequency was observed. Rather the amplitude steadily decreased until about 75° from $\langle 11\bar{2}0\rangle$ it reached an unobservable level. The γ_1^2 frequency was not followed since the values of the neck frequency at crystal symmetry axes and its behavior in its two symmetry planes were all that was needed to determine the pseudopotential model parameters. Very sharp cutoffs were observed in the amplitude of β_3^1 at 4.2° from $\langle 10\bar{1}0\rangle$ and of β_2^2 at 3.5° from $\langle 0001\rangle$, indicating that these orbits have run onto the neck. Cutoffs in the other β oscillations were not observed because their amplitudes dropped rapidly with angle and were obscured by the harmonic content of the α oscillations.

The cyclotron masses m were determined by measuring the temperature dependence of the dHvA amplitude A at a given H. The amplitudes were measured as a function of temperature and the masses were then determined by the least-squares fitting of a straight line to the expression $\ln[(A/T)(1-e^{-2bmT/H})]=-bmT/H$, where b is a known constant (see Lifshitz and Kosevich[15]). The number of points fitted varied from seven to twelve and solutions were obtained iteratively. In this method, the consistency of the mass value can be checked by repeating the process for several different values of the magnetic field. If two frequencies are present this method yields an apparent mass which oscillates at the beat frequency because a single component frequency has been assumed in the calculations. Even when the second frequency has a relatively small amplitude a significant variation may be introduced. In one case, for example, where the amplitude of the second frequency was $2\frac{1}{2}\%$ of the first ($f_2/f_1=1.2$ and $m_2/m_1=0.98$), the apparent mass oscillated with a peak-to-peak variation of 12% of the mean mass.

When using the modulation technique in the presence of two dHvA frequencies, it is possible to null either component over a range of fields by continuous adjustment of the modulation amplitude. However, in this work, the modulation amplitude was not varied with H and therefore the null appeared only at some given field. At neighboring fields the apparent mass

[15] I. M. Lifshitz and A. M. Kosevich, Zh. Eksperim. i Teor. Fiz. **29**, 730 (1955) [English transl.: Soviet Phys.—JETP **2**, 636 (1956)].

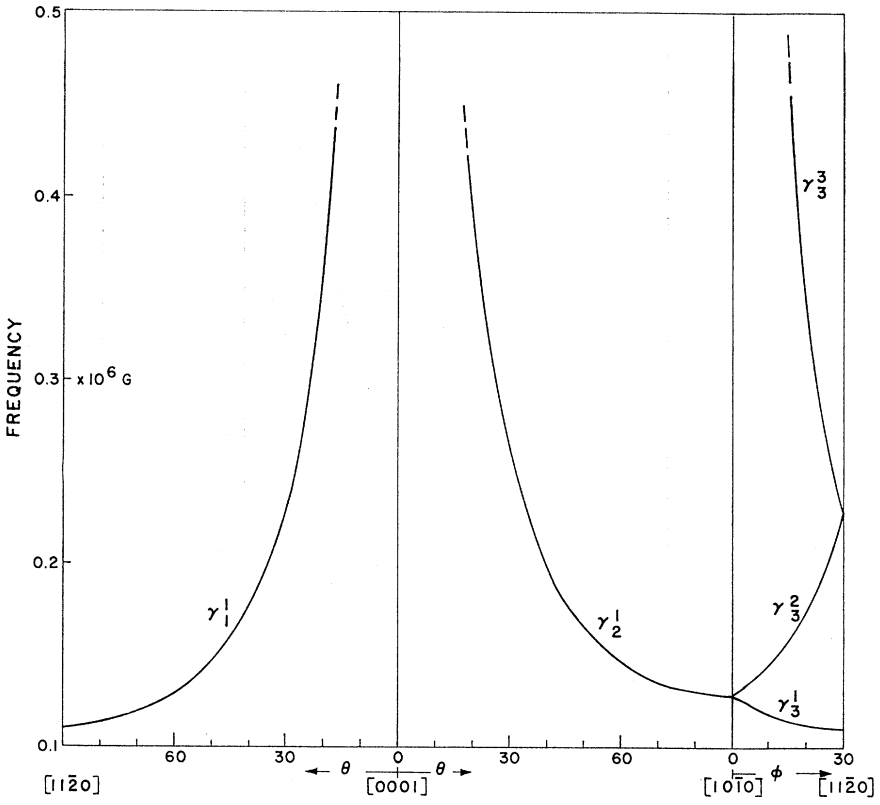

FIG. 4. Linear plot of the angular dependence of the dHvA frequencies arising from orbits on the "neck" of the coronet shown in Fig. 1.

values oscillated with the beat period and the dominant mass was obtained by a simple averaging technique. As the temperature is reduced or the field increased, the harmonic content of a single frequency will introduce significant errors. A narrow band filter was employed to test the resultant signals and data containing more than 1% harmonic content were rejected.

The α_2^1 oscillations provide special problems in mass determinations. Magnetic interaction,[16] even at fields and temperatures where this effect is not severe, introduces a significant amount of second dHvA harmonic which interferes with both the α and β mass determinations. Special techniques which yield the masses in these cases were used.

Suitable choice of detection harmonic and modulation amplitude made it possible to obtain the β_2^2 mass at $\theta=50°$, for example. The α masses themselves were taken at sufficiently low fields and high temperatures that magnetic interaction could be neglected. However, the α^1, α^2 beat pattern is so long that it is not convenient to eliminate one frequency by adjustment of the modulation amplitude. Instead, it was necessary first to separate the component amplitudes by an iterative technique[17] using the observed difference of the component amplitudes at the node field to estimate this difference at the antinode field.

III. PSEUDOPOTENTIAL METHOD

The use of pseudopotentials for calculating band structures[18] is by now sufficiently well known that it suffices here to give a very brief description of the method. The equation satisfied by the pseudo-wave function $|\phi\rangle$ was taken to be

$$\tilde{H}|\phi\rangle\equiv\left\{T+\left[V+\sum_\alpha (E-E_\alpha)\frac{|\alpha\rangle\langle\alpha|}{\langle\alpha|\alpha\rangle}\right]\right\}|\phi\rangle$$
$$=\{T+\tilde{V}\}|\phi\rangle=E|\phi\rangle, \quad (1)$$

using the result $H|\alpha\rangle=\{T+V\}|\alpha\rangle=E_\alpha|\alpha\rangle$, which defines the core level E_α in the lattice, with V the lattice potential and T the kinetic energy. The pseudopotential $\tilde{V}$ depends, in general, not only on position $\mathbf{r}$ but also on the energy E and it is this which gives rise to the expression "nonlocal." Expanding $|\phi\rangle$ in plane waves leads to the usual secular equation. For beryllium with a simple $1s$ core, the matrix elements are

[16] R. D. Plummer and W. L. Gordon, Phys. Rev. Letters **13**, 432 (1964).

[17] P. M. Everett, thesis, Case Western Reserve University, 1968 (unpublished).

[18] W. A. Harrison, *Pseudopotentials in the Theory of Metals* (W. A. Benjamin, Inc., New York, 1966).

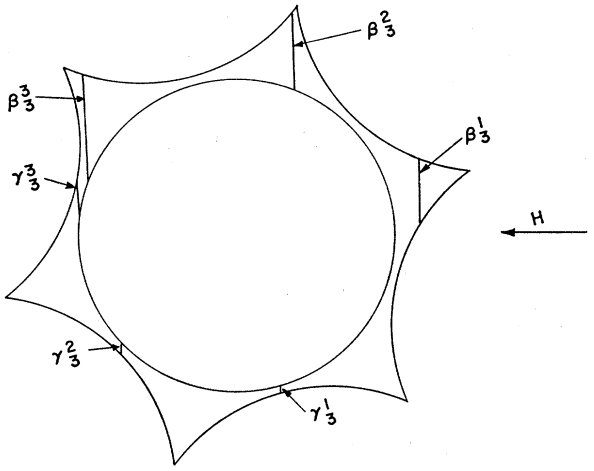

FIG. 5. Cross section of the coronet (not to scale) in the basal plane showing the approximate position of the γ and β orbits for H lying in the basal plane 15° from $\langle 11\bar{2}0\rangle$.

given in atomic units by

$$\tilde{H}_{ij}=k_j^2\delta_{ij}+\frac{1}{\Omega_0}S(\mathbf{G}_{ij})\Big[v(\mathbf{G}_{ij})+[E(\mathbf{k})-E_{1s}]\times\frac{\langle\mathbf{k}_i|1s\rangle\langle 1s|\mathbf{k}_j\rangle}{\langle 1s|1s\rangle}\Big], \quad (2)$$

where $\mathbf{G}_{ij}=\mathbf{k}_i-\mathbf{k}_j$ is a reciprocal lattice vector. Otherwise, $\tilde{H}_{ij}$ vanishes. Ω_0 is the unit cell volume and $S(\mathbf{G}_{ij})$ is the structure factor. If τ_1 and τ_2 are the atomic positions in the unit cell, $S(\mathbf{G})=e^{i\mathbf{G}\cdot\tau_1}+e^{i\mathbf{G}\cdot\tau_2}$. By choosing the origin midway between the two atoms, the structure factors are all real which simplifies the numerical work. Writing the periodic lattice potential V as a sum over all sites of an atomiclike potential $v_{\rm at}(\mathbf{r})$, the term $v(\mathbf{G}_{ij})$ is found to be the Fourier transform:

$$v(\mathbf{G})=\int e^{i\mathbf{G}\cdot\mathbf{r}}v_{\rm at}(\mathbf{r})d\mathbf{r}.$$

Similarly if $\alpha_{1s}(\mathbf{r})$ is the $1s$ atomic orbital

$$\langle 1s|\mathbf{k}\rangle=\int e^{i\mathbf{k}\cdot\mathbf{r}}\alpha_{1s}(\mathbf{r})d\mathbf{r}.$$

E_{1s} is the $1s$ atomic-energy level modified by the presence of the other atoms in the lattice, while $E(\mathbf{k})$ is the eigenvalue of H to be found. The normalization constant $\langle 1s|1s\rangle$ has been included simply to make the expressions independent of the particular normalization used for the atomic functions. It may be seen that the term arising from the nonlocal part of the pseudopotential depends upon $\mathbf{k}_i$ and $\mathbf{k}_j$ separately, whereas, in a local model, the matrix element depends only upon their difference.

TABLE I. Physical properties of pure beryllium.

Lattice dimensions at 0°K[a]	$c=3.5814$ Å
	$a=2.2828$ Å
Unit cell volume at 0°K	$\Omega_0=109.0758$ (a.u.)^3
Brillouin-zone dimensions	$\Gamma A=0.4642$ (a.u.)$^{-1}$
	$\Gamma K=0.9710$ (a.u.)$^{-1}$
Radius of the free-electron sphere	$k_F=1.0278$ (a.u.)$^{-1}$
Elastic constants at 0°K[b]	$C_{11}=29.94$
in units of 10^{11} dyn/cm^2	$C_{12}=2.76$
	$C_{13}=1.1$
	$C_{33}=34.22$
	$C_{44}=16.62$
Work function[c]	0.23 Ry
Free-atom $1s$ level[d]	8.698 Ry
Number of states/atom contained in the hole or electron surfaces (calc.)	0.01573
Density of states at Fermi level (calc.)	0.85 states/atom Ry
(expt.)[e]	0.99 states/atom Ry

[a] References 19 and 20.
[b] J. F. Smith and C. L. Arbogast, J. Appl. Phys. **31**, 99 (1960).
[c] R. Schulze, Z. Physik **92**, 212 (1934).
[d] Reference 21.
[e] G. Ahlers, Phys. Rev. **145**, 419 (1966). This value supersedes that quoted in Ref. 7.

IV. CALCULATION

Equation (2) provides the formal recipe for calculating the energy levels as a function of position in the Brillouin zone. The Fermi surface is then constructed to enclose a volume twice that of the zone and dHvA frequencies found by evaluating extremal cross sections of the Fermi surface. The density-of-states curve and effective cyclotron masses on the Fermi surface may also be found.

It is important to notice from Eq. (2) that the eigenvalue $E(\mathbf{k})$ itself appears in the matrix elements and therefore must be found self-consistently. There is no serious problem on a surface of constant energy, where one is interested in $\mathbf{k}$ as a function of E, and in any case convergence of the iteration is very rapid.

The errors which arise from truncating the expansion of the pseudo-wave function may be minimized by the correct choice of plane waves included in the combination. Symmetry considerations suggest that, at least near the Fermi level, these errors are smaller if 12 rather than, say, 11 or 13 waves are used. The next smallest number would be 24.

The final results depend sensitively on the lattice constants c and a which in the present work (see Table I) were taken from Ref. 19 and corrected for temperature using the thermal expansion data of Ref. 20. The atomic orbital α_{1s} is taken as the free-atom wave function, tabulated in Ref. 21.

To complete the setting up of a matrix element it is necessary to know the potential $v_{\rm at}(\mathbf{r})$ and also the shifted atomic core level E_{1s}. Following the method of Ref. 22, the coefficients $v(G)$ which depend only on the

[19] G. London (private communication).
[20] R. W. Meyerhoff and J. P. Smith, J. Appl. Phys. **33**, 219 (1962).
[21] F. Herman and S. Skillman, *Atomic Structure Calculations* (Prentice-Hall, Inc., Englewood Cliffs, N. J., 1963).
[22] J. C. Kimball, R. W. Stark, and F. M. Mueller, Phys. Rev. **162**, 600 (1967).

magnitude of **G** are treated together with E_{1s} as disposable parameters chosen to minimize the deviations between calculated and observed dHvA frequencies. Since results are sensitive only to the shorter **G** vectors, it is possible to determine accurately only four values of $v(G)$ corresponding to the vectors $10\bar{1}0$, 0002, $10\bar{1}1$, and $10\bar{1}2$. The value of $v(0001)$ does not affect the results because $S(0001)$ vanishes while $v(0)$ simply fixes the zero of energy: Neither is given by this method. For the longer **G** vectors, the off-diagonal elements are set to zero, equivalent to assuming exact cancellation between the local and nonlocal parts of the pseudopotential.

There are several salient features of the experimental Fermi-surface results which are of great use in guiding the procedure for frequency fitting (see Figs. 3 and 4). The first and most obvious is the absence of pockets of electrons, both at Γ (the lens) and at L (butterflies and needles) which in an empty lattice model would be present. In the earliest stages of fitting, this rules out certain combinations of parameters immediately. Having removed these unwanted pieces of the Fermi surface the next feature to notice is that the necks connecting up the coronet are very thin and have a low effective mass. These γ frequencies are sensitive to all the parameters and thus act as effective constraints. Another distinctive observation is the appearance of the beat frequency $\alpha^2-\alpha^1$ in the cigar oscillations. Only for restricted ranges of the parameter values does this waisting in the cigar occur in the model. It turns out that the beat frequency is particularly sensitive to the energy difference $(E-E_{1s})$ in the nonlocal term. It also depends upon the energy at which the T_1 and T_4 bands cross each other near K on the ΓK axis (see Sec. V). It seems that good agreement is obtained only when this crossing lies below the Fermi level, so that T_1 defines the ΓK dimension of the cigar while T_4 defines the coronet. With these general considerations in mind, the fitting procedure for the dHvA frequencies was considerably expedited.

V. RESULTS AND DISCUSSION

Some relevant data for pure beryllium are shown in Table I, while in Table II the final values of the fitted pseudopotential are listed and compared with other possible forms of the potential. It is worth mentioning here that the pseudopotential fitted in the way described is not necessarily unique and neither is it altogether independent of the numerical procedures used in the calculation. For example, small changes would be required if a different number of plane waves were used in the expansion. The second column in Table II gives values of the Fourier transform of the self-consistent potential used by Loucks and Cutler in their orthogonalized plane-wave (OPW) calculation.[1] Since the pseudopotential and OPW formulations are essentially identical, the potentials should be comparable and

TABLE II. Comparison of potential coefficients used in beryllium calculations. Values of $v(\mathbf{G})/\Omega_0$ are given in Ry.

G	Present work	Loucks and Cutler	Local approx.[a]	Heine and Animalu[b]
$10\bar{1}0$	−0.1947	−0.1809	0.0571	0.0334
0002	−0.1630	−0.1587	0.0889	0.0470
$10\bar{1}1$	−0.1537	−0.1513	0.0981	0.0479
$10\bar{1}2$	−0.1163	−0.1009	0.0976	0.0318
0000	−0.62[c]			−0.352
E_F-E_{1s}	8.64			

[a] Obtained from the full nonlocal matrix element [Eq. (2)] where both states lie on the Fermi sphere.
[b] Note that these values have been normalized to the unit cell volume Ω_0.
[c] Estimated, using the experimental work function of beryllium.

indeed it appears that the average difference between the two is only 0.009 Ry. If the nonlocal term in the pseudopotential Eq. (2) is evaluated with both states on the Fermi sphere, free-electron radius k_F, and added to the local term, then the resulting local-type potential should be comparable with the form factor derived from the model potential by Animalu and Heine.[23] (For $G>2k_F$, initial and final states are antiparallel.) The comparison is shown in the last two columns of Table II and for the three Brillouin-zone planes intersecting the Fermi surface, there is a factor of almost 2 between them. This difference seems to have no simple explanation. A glance at columns one and three shows that the cancellation of the crystal potential by the orthogonalization terms in Eq. (2) reduces the strength of the net potential by a factor of 2 or 3. However, a brief investigation of such a local form indicated that not only was quantitative agreement with experiment poor, but also the unwanted pieces of the Fermi surface (lens, butterflies) appeared. If beryllium behaves in this respect at all like magnesium,[22] then a local fit might be expected to be inferior. The value of $v(0)$ in the table was estimated from the experimental work function of beryllium. The energy difference E_F-E_{1s} used in the calculation 8.64 Ry lies close to the value it would assume if the free-atom level were unaffected by the presence of neighbors in the crystal, namely, 8.46 Ry.

In Table III some calculated dHvA frequencies are compared both with our own observed values and also with those of Watts. Corresponding cyclotron masses are included in this table. The high accuracy of those frequencies used in the parameter fitting process is maintained for other directions of the magnetic field, as may be seen in Table III. It is encouraging that even though the potential can distort the free-electron sphere enough to exclude the smaller overlaps into higher Brillouin zones, yet the model agrees so well with experiment: In symmetry directions the agreement is better than 1%. Following the frequency branches out from the symmetry axes, this accuracy is maintained except for the sensitive γ frequencies. Even here the deviations increase only to about $2\frac{1}{2}$%. The number of electron states per atom in the cigar is equal to the

[23] A. O. E. Animalu and V. Heine, Phil. Mag. 12, 1249 (1965).

TABLE III. Calculated and observed dHvA frequencies and the corresponding cyclotron masses. Frequencies are in units of 10^6 G while masses are relative to a free-electron mass of 1. The last column shows the mass enhancement factor.

Field direction θ, and branch		dHvA frequencies Present calculation	Present experiment	% diff.	Watts expt.	Cyclotron masses Present (calc.)	Present (expt.[a])	Expt./calc.
Cigar								
α^1	0°	9.48[b]	9.42	0.6	9.55	0.136	0.168	1.24
α^2	0°	9.75[b]	9.72	0.3	9.85	0.142	0.170	1.20
α_2^1	20°	10.14	10.07	0.7		0.145	0.180	1.24
α_2^2	20°	10.35	10.31	0.4		0.151	0.180	1.19
α_2^2	50°	14.92	14.90	0.1		0.213	0.251	1.18
α_2^2	90°	53.77[b]	54.0	−0.4	53.7	0.496		
α_1^2	90°	53.08	53.1	0.04	53.7	0.491		
Coronet								
γ_1^1	90°	0.1097[b]	0.110	−0.3	0.113	−0.0178	−0.0212	1.18
γ_1^1	78.6°	0.1119	0.112	−0.1		−0.0182	−0.0215	1.18
γ_1^1	70.1°	0.1167	0.116	0.6		−0.0190	−0.0223	1.17
γ_1^1	60.6°	0.1262	0.127	−0.6		−0.0205	−0.0240	1.17
γ_1^1	54.5°	0.1353	0.138	−1.9		−0.0220	−0.0259	1.18
γ_1^1	50.6°	0.1428	0.146	−2.2		−0.0233		
γ_1^2	90°	0.2257	0.226	−0.1	0.23	−0.0372		
γ_2^1	90°	0.1270	0.127	0.0	0.131	−0.0207		
β_1^1	90°	12.41	12.4	0.1	12.5	−0.214	−0.260	1.22
β_1^2	90°	15.31	15.3	0.1	15.4	−0.298	−0.35±0.02	1.17
β_2^2	90°	14.86[b]	14.91	−0.3	15.0	−0.285	−0.35±0.03	1.23
β_2^2	85°	14.64	14.60	0.3		−0.273	−0.33±0.02	1.21
β_2^2	75°	13.74	13.68	0.4		−0.237	−0.285	1.20
β_2^2	65°	13.06	12.98	0.6		−0.215	−0.256	1.19
β_2^2	52°	12.75	12.65	0.8		−0.203	−0.256	1.26
λ^1	0°	393.8			381	1.021		
λ^2	0°	528.1				−1.405		

[a] The uncertainty in masses is estimated to be ±3% except where specifically stated.
[b] Used in the frequency fitting procedure.

number of hole states per atom in the coronet, calculated to be 0.01573.

The situation with regard to the masses shows no such good agreement and it is generally accepted (see Ref. 18, p. 125, for example) that the observed masses are enhanced by electron-electron and electron-phonon interactions neglected in the present treatment. Within experimental uncertainties the enhancement factors shown in the last column of Table III are essentially constant. We feel that these values are more reliable than the preliminary ones given in Ref. 7. The enhancement factor is in rough agreement with a comparison of the calculated density of states at the Fermi level, 0.85 states/Ry atom, to the value from specific heat measurements on high purity beryllium of 0.99 states/Ry atom (see Table I). where the factor is 1.16. Note that this differs from the specific heat enhancement quoted in Ref. 7, being based on an improved determination of the specific heat.

TABLE IV. Calculated caliper dimensions of the Fermi surface in $(\text{a.u.})^{-1}$ (see Fig. 2 for designations).

Caliper	Present calc.	Watts[a]	Loucks[b]	Terrell[c]
Ka	0.1317	0.09(0)	0.141	0.190
Kb	0.0711	0.09(0)	0.075	
rc	0.1239	0.09(2)		0.185
rd	0.0728	0.09(2)		
Kr	0.129			
Ke	0.4288	0.48	0.453	0.465
Γ*l*	0.5777	0.56	0.574	0.59
Γ*g*	0.762			
lk	0.2518	0.23	0.246	0.23
gh	0.108	0.13	0.118	
Γ*n*	0.5796	0.57		0.58
Γ*p*	0.590			
no	0.0196	0.02	0.017	0.01
pq	0.0095			
ak	0.0098	0.08	0.008	

[a] Reference 5.
[b] Reference 2.
[c] J. H. Terrell, Phys. Letters **8**, 149 (1964).

In earlier first principles calculations,[1–3] there was general qualitative agreement between predicted and observed values for large extremal cross sections of the Fermi surface but they failed to fit the finer details of the surface. This is probably due to the sensitivity of these features to the choice of potential. These points are well illustrated by Table IV where caliper dimensions for this model and previous models are compared.

An important point to note from Table IV is the height *je* of the cigar (see Fig. 2). The Brillouin-zone height is 0.4642 $(\text{a.u.})^{-1}$ so that while the cigar constructed by Watts actually overlapped the zone boundary and contained open orbits the present model cigar does not. However, as Watts has pointed out, the two cases are not experimentally distinguishable on the basis, for example, of magnetoresistance saturation because even at fields of the order of one gauss there is magnetic breakdown across the *AHL* zone face. Watts's cigar height was based on an assumed circular waist section of the cigar, whereas all calculations have subsequently indicated a triangular section. The present

TABLE V. Symmetry point energies relative to Γ_1^+ in Ry.

	Present calc.	Terrell
Γ_1^+	0	0
Γ_4^-	0.9132	0.8999
Γ_3^+	0.5548	0.5185
M_1^+	0.4998	0.4644
M_2^-	0.6180	0.6048
M_2^-	1.4373	1.2919
M_3^+	1.3222	1.2996
M_4^-	1.1847	1.0962
K_6	1.4204	1.3132
K_1	0.7004	0.6415
K_5	0.7871	0.7605
L_1	0.6075	0.5729
L_1	0.9614	0.9278
H_1	0.9109	0.8463
H_2	1.3422	1.2563
H_3	0.7927	0.7588
A_1	0.1642	0.1612
A_1	1.7253	1.5945
E_F	0.8796	0.84
T_1,T_4 crossing	0.8611	

work gives a value for the radius of curvature at the corners of the triangle (along ΓK) of 0.002 (a.u.)$^{-1}$.

This last result can be used in estimating a value for the breakdown field for electrons moving around the waist of the cigar with the magnetic field along the c axis. Using the curvatures of both cigar and coronet on the ΓK axis, together with the distance in reciprocal space, ak, in Fig. 2, across which the electrons must tunnel to reach the coronet, the breakdown field obtained[24] is about 120 kG. This value is of the right order to explain the onset of magnetic breakdown observed by Watts in fields approaching 100 kG, although no detailed fit to his data has been attempted. This breakdown has also been observed in the magnetoresistance measurements of Alekseevski *et al.*[25] where a departure from the usual parabolic field dependence begins around 50 kG.[26]

A comparison of the energy levels at symmetry points with those of Terrell[3] is given in Table V. Terrell's $E(\mathbf{k})$ curves have a slope on the average 6% smaller than our own which indicates that effective masses in Terrell's calculation are 6% higher than ours. Correspondingly, the mass enhancement factors are reduced. Energy values along symmetry directions have been computed self-consistently and are shown in Fig. 6.

In a semiempirical model of this type, it is difficult to estimate the "accuracy" since the discrepancies between calculated and measured frequencies are themselves used to determine the potential. However, it is important to know how well the Fermi level can be found using the volume of the Fermi surface as the

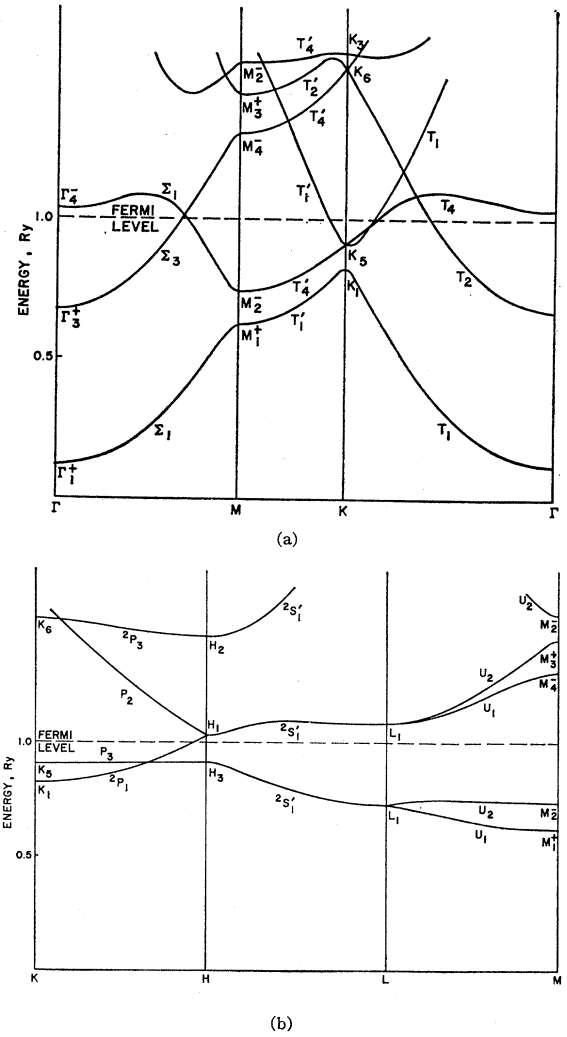

FIG. 6. Self-consistent energy eigenvalues for the major symmetry axes.

criterion, because in applying the model to strained lattices, this level becomes the only quantity to be determined. Now, the model is effectively insensitive to changes in E_F small enough to maintain the accuracy of the selected frequencies, roughly $\frac{1}{2}$%. The uncertainty in E_F is thus set by the neck orbit, since this has the lowest effective mass. In this case a frequency shift of 0.4% is produced by a change of 20 μRy which provides a reasonable estimate of the uncertainty in E_F.

VI. EFFECTS OF STRAIN

As long as any strains in the lattice preserve hexagonal symmetry, there is no difficulty in applying the model of pure beryllium to the determination of the strain dependence of the band structure, and the strain and pressure derivatives of dHvA frequencies may be calculated. The present work treats only displacements in this class, including uniaxial strain along the c axis

[24] R. G. Chambers, Proc. Phys. Soc. (London) **88**, 701 (1966).
[25] N. E. Alekseevski, V. S. Egorov, and A. V. Dubrovin, Zh. Eksperim. i Teor. Fiz. Pis'ma v Redaktsiyu **6**, 793 (1967) [English transl.: Soviet Phys.—JETP Letters **6**, 249 (1967)].
[26] N. E. Alekseevski (private communication). Because of an error of $\frac{1}{2}\pi$ in the field orientation shown in Fig. 1 of Ref. 25, the breakdown observed is between cigar waist and coronet and not between the ends of cigars as the figure implies. This latter breakdown would require very much higher field strengths.

TABLE VI. Experimental and theoretical values of pressure derivatives of dHvA frequencies. Values of $\partial \ln f/\partial p$ are given in units of 10^{-4} kbar^{-1} where f is the frequency and p is the pressure.

Sheet	Field direction	Present calc.	O'Sullivan and Schirber
Cigar			
α^1	$\langle 0001\rangle$	$-1.9\pm$ 1.0	$-1.0\pm$ 0.6
α^2	$\langle 0001\rangle$	$1.7\pm$ 1.0	$1.6\pm$ 0.4
Coronet			
γ^1	$\langle 11\bar{2}0\rangle$	-15.0 ± 12	-40 ±10
β^1	$\langle 11\bar{2}0\rangle$	$3.5\pm$ 1.4	3 ±1
β^2	$\langle 10\bar{1}0\rangle$	$5.5\pm$ 1.3	

of the crystal and the strain field corresponding to hydrostatic pressure.

Clearly, it is of first importance to know how the crystal potential changes with lattice spacings, c and a. In a first-principles calculation, it is usually possible to find how the several contributions to the potential, such as the ion core, exchange, etc., each vary. Even in a model potential of the Heine-Abarenkov type, the pressure dependence is known.[27] In this semiempirical model, however, the potential is available only as a number of Fourier components $v(G)$ of the local part of a pseudopotential. The simplest assumption, and the one used here, is that $v(G)$ is a smooth function of G. Values appropriate to the changed reciprocal lattice vector magnitudes may then be interpolated. The core level E_{1s} which also appears in the pseudopotential is kept fixed in this treatment. The explicit dependence of the matrix elements, Eq. (2), on cell volume is included in the computation.

For the case of hydrostatic pressure, values of c and a are obtained from the data in Table I and the changes

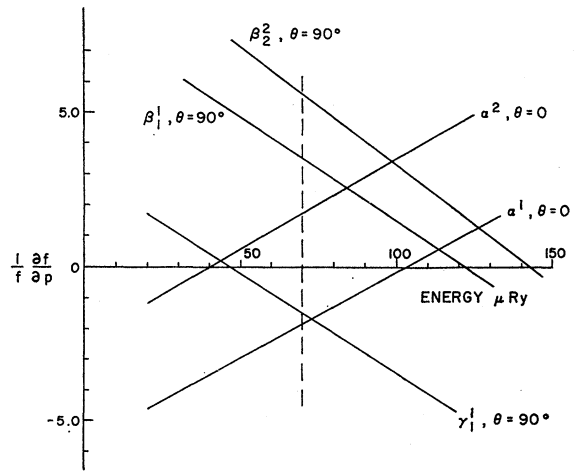

FIG. 7. Variation of $\partial \ln f/\partial p$ with estimated Fermi level for various frequencies f. For γ_1^1 the ordinate is in units of 10^{-3} kbar^{-1} and for all other frequencies 10^{-4} kbar^{-1}. The correct Fermi level on this energy scale is 70 μRy and is indicated by the vertical dashed line.

[27] B. Vasvari, A. O. E. Animalu, and V. Heine, Phys. Rev. **154**, 535 (1967); A. O. E. Animalu (private communication).

TABLE VII. Theoretical values of strain derivatives of dHvA frequencies. Values of $\partial \ln f/\partial \epsilon_3$ are given, where ϵ_3 is the strain along the c axis.

Sheet	Field direction	Present calc.
Cigar		
α^1	$\langle 0001\rangle$	-2.1 ± 0.5
α^2	$\langle 0001\rangle$	-2.2 ± 0.5
Coronet		
γ^1	$\langle 1120\rangle$	-100 ±5

in pseudopotential are found as outlined above. The derivatives are then obtained from the dHvA frequency differences. The Fermi level for the compressed metal is found as before by equating the numbers of hole and electron states. To achieve this, the Fermi energy is estimated and the volumes of the corresponding hole and electron surfaces are compared. From the density of states the true value of E_F can then be obtained. Figure 7 shows how the calculated pressure derivatives vary with the estimated Fermi level. It is at once apparent that a correction to the level of 20 μRy, which is the estimated uncertainty in the calculation, would produce a considerable fractional change in the derivative values. In particular, the γ_1^1 derivative varies some ten times more rapidly than the other frequencies because of its small effective mass.

From Fig. 7, using the best estimate of E_F, the pressure derivatives can be obtained. The results are shown in Table VI. The available data of O'Sullivan and Schirber[28] are in good agreement for the $\alpha^{1,2}$ and β^1 frequencies, but there is a discrepancy between calculated and observed values for γ_1^1. However, despite the great sensitivity of this frequency to all the parameters, the difference lies only just outside the range of the combined estimated errors. It is of some interest that both experimentally and theoretically the α^1 and α^2 frequencies change in opposite directions with pressure, but a shift of only 30 μRy would suffice to make both the calculated values assume the same sign. If the pressure dependence were linear over a sufficiently large range, the beat frequency would vanish completely at a negative pressure (tension) of about 100 kbar. At tensions of this order, the model also predicts the appearance of a small lens portion of the Fermi surface, but well before this, the cigar will touch the coronet along ΓK, changing the topology of observable orbits on the surface. The pressure at which this happens is also the pressure at which the T_1 and T_4 levels near K on ΓK cross at the Fermi level itself. Table V shows that in the unstrained metal this crossing lies only a few hundredths of a Ry below E_F.

Some strain derivatives for uniform strain along the c axis have also been calculated and presented in Table VII. In the absence of comparable experimental data, these values must be regarded as predictions.

[28] W. J. O'Sullivan and J. E. Schirber, Phys. Letters **25A**, 124 (1967); and private communication.

VII. CONCLUSION

It has been shown how a nonlocal pseudopotential can be set up and parameterized in such a way as to give a very precise description of the Fermi surface of beryllium. Calculated and observed dHvA frequencies agree in most cases to within 1%. The effective masses computed for the various orbits indicate an electron mass enhancement due to many-body interactions of about 20%. The model also provides much other useful information on the behavior of electrons in beryllium. For example, the detailed knowledge of the shape of the Fermi surface yields caliper dimensions and allows some understanding of magnetic breakdown between orbits. The electronic specific heat also comes out of the calculation.

Further uses of the model include adapting it for computing pressure and strain variations of the band structure. With increased precision in calculation and alternative assumptions concerning the changes in pseudopotential under conditions of strain, the agreement with experimental values should improve, since the present approach yields reasonable results. Finally, this model may also be applied to the case of dilute alloys where the simplest procedure is to combine the effects of lattice-dimension changes with changes in the Fermi surface due to variation in electron density. Within this approximation, the Fermi-surface topology is more easily changed by altering the electron concentration than by application of pressure alone. This interesting problem remains to be discussed in a later publication.

ACKNOWLEDGMENTS

The authors gratefully acknowledge the assistance of Dr. D. Parsons and J. M. Fiske, and the helpful suggestions of Dr. J. P. G. Shepherd and Dr. Alex Animalu.

PHYSICAL REVIEW VOLUME 180, NUMBER 3 15 APRIL 1969

Magnetoconductivity of a Fermi Ellipsoid with Anisotropic Relaxation Time

H. J. MACKEY AND J. R. SYBERT
Department of Physics, North Texas State University, Denton, Texas 76203
(Received 28 October 1968)

An extremely simple expression is obtained for the isothermal conductivity tensor for an arbitrarily oriented Fermi ellipsoid in an arbitrarily oriented magnetic field. The relationship between a simple kinetic equation and a vector form of the Boltzmann equation is demonstrated, and this relationship is used to show how to include the relaxation time as a tensor quantity. One again obtains a simple result which possesses the general characteristics shown to be required by other workers dealing in a different approximation.

INTRODUCTION

IN a previous paper,[1] the authors have utilized the Ham-Mattis transformation[2] to obtain a tensor relationship between the kinetic coefficients of electron transport calculated for an arbitrarily oriented Fermi ellipsoid with magnetic field **H** directed along the 3 axis and the corresponding coefficients calculated for a Fermi sphere with **H** along the 3 axis. The resulting expressions are functions of the elements of the reciprocal effective-mass tensor $\hat{\alpha}=\hat{m}^{-1}$ and the magnitude of **H**. This paper discusses the form taken by the isothermal-conductivity tensor $\hat{\sigma}$ of an arbitrarily oriented Fermi ellipsoid with **H** not restricted to any specific direction relative to experimental coordinates. The result is of an extremely simple form and is a function of the elements of the mass tensor $\hat{m}$ directly along with the components of **H**. Herring and Vogt[3] have treated the problem of allowing for anisotropy in the scattering by introducing tensor relaxation times $\hat{\tau}^{(i)}$, defined for each ellipsoidal piece of the Fermi surface such that $\hat{\tau}^{(i)}$ is simultaneously diagonal with its corresponding mass tensor $\hat{m}^{(i)}$. Working in this approximation with emphasis on Maxwellian distributions, they have shown that the diagonal elements $m^{(i)}{}_{jj}$, which occur in isotropic scalar τ theory, are simply replaced by $m^{(i)}{}_{jj}/\tau^{(i)}{}_{jj}$; i.e., the tensor $\hat{\tau}$ formalism weights the diagonal mass elements with corresponding $\hat{\tau}$ elements. They obtain expressions for the various conductivity elements by an iterative technique which generates a series valid at low magnetic field. The present paper deals with a highly degenerate system at very low temperatures such that emphasis is on a Fermi distribution. Hence the results are applicable to the metals and semimetals. In the present approximation, results are obtained in closed form, valid for all values of magnetic field. Korenblit[4] has dealt with the case where there is a single $\hat{\tau}$ seen by all the ellipsoids such that $\hat{\tau}$ does not belong to the principal axes of any ellipsoid. He has shown how to introduce $\hat{\tau}$ directly into the Boltzmann equation. The present work indicates how this modified Boltzmann equation may be reduced

[1] H. J. Mackey and J. R. Sybert, Phys. Rev. **172**, 603 (1968).
[2] F. S. Ham and D. C. Mattis, IBM J. Res. Develop. **4**, 143 (1960).
[3] C. Herring and E. Vogt, Phys. Rev. **101**, 944 (1956).
[4] I. Ya. Korenblit, Fiz. Tverd. Tela **2**, 3083 (1960) [English transl.: Soviet Phys.—Solid State **2**, 2738 (1961)].